

Deformable spin- $\frac{1}{2}$ XX chain with three-site interactions at zero and finite temperatures

Oleg Derzhko,^{1,2} Taras Krokhamlskii,^{1,2} Joachim Stolze,² and Taras Verkholyak¹

¹*Institute for Condensed Matter Physics, National Academy of Sciences of Ukraine, 1 Svientsitskii Street, L'viv-11, 79011, Ukraine*

²*Institut für Physik, Technische Universität Dortmund, 44221, Dortmund, Germany*

(Received 7 November 2008; revised manuscript received 4 February 2009; published 11 March 2009)

We study spin-Peierls structural lattice instabilities for a spin-1/2 isotropic XY chain with three-site interactions of $(XZX+YZY)$ type. Within the adopted adiabatic treatment we have to examine the ground-state energy or the Helmholtz free energy of the spin chain with exchange couplings varying coherently with a possible static lattice distortion pattern. Since the considered spin model can be converted into a system of noninteracting spinless fermions the required ground-state energy or the Helmholtz free energy can be calculated accurately without making any approximations. We examine rigorously several lattice distortion patterns focusing on dimerized and trimerized ones, which owe their presence to the spin-Peierls mechanism. We present phase diagrams illustrating the effect of the three-site interaction on the spin-Peierls lattice distortions. Finally we discuss some properties of the deformable spin chain in the ground state and at finite temperatures. In particular, we examine the transverse magnetization, the static transverse susceptibility and the specific heat illustrating the changes in these quantities due to lattice instabilities.

DOI: 10.1103/PhysRevB.79.094410

PACS number(s): 75.10.-b

I. INTRODUCTION: THE MODEL

Quantum spin systems with multisite interactions have attracted much interest during the past decade. Such systems emerge naturally as effective spin models for the standard Hubbard model at half filling in higher orders of the strong-coupling t/U expansion¹ (see also Refs. 2 and 3). Another example is provided by quantum spin systems with energy currents.⁴ The presence of multisite interactions may produce competition between different interactions and therefore may have a noticeable influence on the properties of the spin systems especially at low temperatures and in low dimensions. Exactly solvable quantum spin models with multisite interactions, in which effects of multisite interactions can be followed reliably, are of particular interest. As an example we may mention here one-dimensional modified XXZ models with competing interactions which exhibit incommensurate behavior and which can be examined accurately using the Bethe ansatz approach.⁵ Another class of models is based on the Jordan-Wigner fermionization approach.⁶ After applying the Jordan-Wigner transformation some quantum spin chains with multisite interactions may be converted into systems of noninteracting spinless fermions, and hence they admit a rigorous analysis.⁷⁻¹¹

In the present study we consider a particular model with multisite interactions belonging to the free-fermion class.^{9,10} Our goal is to examine spin-Peierls phenomena within an adiabatic treatment. Note that our purpose is not to model any specific material, but simply to study accurately a model amenable to rigorous calculations. The present work may be a vehicle for further studies of more complicated quantum chains.

More specifically, we consider a spin-1/2 chain with isotropic XY (i.e., XX) interaction between neighboring sites and $XZX+YZY$ interaction between three contiguous sites. The Hamiltonian of the model on a lattice of N sites reads

$$H = \sum_{n=1}^N [J(s_n^x s_{n+1}^x + s_n^y s_{n+1}^y) + K(s_n^x s_{n+1}^z s_{n+2}^x + s_n^y s_{n+1}^z s_{n+2}^y)], \quad (1)$$

where J and K are the two-site and the three-site couplings between the sites n and $n+1$ and between the sites $n, n+1$, and $n+2$, respectively. The particular boundary conditions imposed are not essential for the thermodynamic quantities which are studied below in the limit $N \rightarrow \infty$. We also note that the thermodynamic quantities are insensitive to the sign of the couplings J and K since the sign of J or K may be changed by an appropriate unitary transformation. The merit of the spin model considered is its exact solvability: After applying the Jordan-Wigner transformation¹² it reduces to a one-dimensional model of spinless fermions with nearest-neighbor and next-nearest-neighbor hoppings. From Ref. 10 we know that spin model (1) exhibits two different spin-liquid phases separated by a quantum phase transition at the critical value of the three-site interaction strength $K_{\text{crit}} = \pm 2|J|$.

To discuss spin-Peierls phenomena within an adiabatic treatment we have to assume a (trial) static lattice distortion which can be characterized by a set $\{\delta_n\}$, where $\delta_n = \epsilon_{n+1} - \epsilon_n$ is the (dimensionless) change in the distance between the sites n and $n+1$, ϵ_n is the (dimensionless) displacement of the site n , and $\sum_{n=1}^N \delta_n = 0$ (fixed-length case). Since exchange couplings in spin models are related to matrix elements between electronic states, such a change obviously leads to exchange couplings $J \rightarrow J_n$ and $K \rightarrow K_n$ in Eq. (1). We assume a linear dependence of the couplings on the intersite distance changes $\{\delta_n\}$:

$$J_n = J(1 - \delta_n), \quad K_n = K(1 - \aleph \delta_n - \aleph \delta_{n+1}). \quad (2)$$

Moreover, we assume that K_n depends explicitly on δ_n and δ_{n+1} only, and the parameter \aleph is introduced to distinguish between the effects of intersite distance change on the two-site and the three-site interactions. In what follows we set

$\aleph=1$ for simplicity. For the case of pure dimerization, $\delta_n + \delta_{n+1}=0$ and K_n will depend neither on n nor on $|\delta_n|$. This does not imply, however, that the three-site coupling K becomes irrelevant.

Using the Jordan-Wigner fermionization approach one can calculate accurately¹² the ground-state energy of the spin system $E_0(\{\delta_n\})$ (zero-temperature case) or the Helmholtz free energy of the spin system $F(\{\delta_n\})$ (finite-temperature case). The total ground-state energy $N\mathcal{E}(\{\delta_n\})$ [Helmholtz free energy $N\mathcal{F}(\{\delta_n\})$] consists of the magnetic part $E_0(\{\delta_n\})[F(\{\delta_n\})]$ and the elastic part $\alpha\sum_{n=1}^N\delta_n^2$, where α is an elastic constant. The further analysis proceeds along standard lines: finding the lowest-energy lattice pattern comparing (usually a restricted number of) trial lattice patterns.

The aim of the present study is to examine the role of the three-site interactions, which come into play when $K \neq 0$. We recall that for $K=0$ the dimerized pattern [i.e., $\delta_n=(-1)^n\delta$] is known^{13,14} to yield a lower energy than that of the uniform chain (i.e., $\delta_n=0$). More complicated lattice patterns may become favorable in comparison with the uniform one in the presence of an external (transverse) magnetic field.¹⁵⁻¹⁸ The effect of the three-site interactions on the spin-Peierls instability has not been studied until now, while there exist similar studies on the effect of two-site next-nearest-neighbor exchange interactions on spin-Peierls chains.¹⁹⁻²² With our paper, we attempt to fill this gap. Some preliminary results of the present study were announced in Ref. 23.

The rest of the paper is organized as follows. In Sec. II we report some exact calculations for periodically distorted spin-1/2 XX chains with three-site interactions focusing on the period-2 and period-3 cases. We use these results to construct phase diagrams in Sec. III. Knowing the phase diagrams we can calculate various quantities characterizing the deformable spin chain at zero and finite temperatures (Sec. IV). In particular, we examine the dependence of the transverse magnetization on the strength of the three-site interaction K at different temperatures and the temperature dependences of the energy gap, the static transverse susceptibility, and the specific heat at various values of K . Finally, we summarize our findings in Sec. V.

II. PERIODIC SPIN CHAINS

In this section we compute rigorously the ground-state energy and the Helmholtz free energy of some periodic spin chains which correspond to trial lattice dimerization/trimerization patterns. For this purpose we consider an inhomogeneous version of Hamiltonian (1) (i.e., $J \rightarrow J_n$, $K \rightarrow K_n$) and assume a periodic sequence of the couplings of period $p, \dots, J_1K_1J_2K_2 \dots J_pK_pJ_1K_1J_2K_2 \dots J_pK_p \dots$. After performing the Jordan-Wigner transformation¹² we arrive at a (periodic) system of spinless fermions on a chain with nearest-neighbor and next-nearest-neighbor hoppings

$$H = \sum_{n=1}^N \left[\frac{J_n}{2} (c_n^\dagger c_{n+1} + c_{n+1}^\dagger c_n) - \frac{K_n}{4} (c_n^\dagger c_{n+2} + c_{n+2}^\dagger c_n) \right]. \quad (3)$$

For the calculation of thermodynamic quantities in the limit $N \rightarrow \infty$ we may assume periodic boundary conditions in Eq.

(3). The Hamiltonian of spinless fermions (3) after some straightforward manipulations can be further brought to a diagonal form

$$H = \sum_{i=1}^p \sum_{\kappa} \Lambda_{i,\kappa} \eta_{i,\kappa}^\dagger \eta_{i,\kappa} \quad (4)$$

with $\kappa=2\pi n/\mathcal{N}$, $n=-\mathcal{N}/2, -\mathcal{N}/2+1, \dots, \mathcal{N}/2-1$. We assume $\mathcal{N}=N/p$ to be even.

For a chain with period $p=2$ we have an explicit expression for the spinless fermion energies,

$$\begin{aligned} \Lambda_{i,\kappa} = & -\frac{K_1+K_2}{4} \cos \kappa \\ & \pm \frac{1}{2} \sqrt{\left(\frac{K_1-K_2}{2} \cos \kappa\right)^2 + J_1^2 + J_2^2 + 2J_1J_2 \cos \kappa} \end{aligned} \quad (5)$$

(see also Ref. 24).

For a period-3 chain the energies $\Lambda_{i,\kappa}$ are the three solutions of the cubic equation $\Lambda_{i,\kappa}^3 + A\Lambda_{i,\kappa} + B=0$ with

$$\begin{aligned} A = & \frac{J_1K_2 + J_2K_3 + J_3K_1}{4} \cos \kappa - \frac{J_1^2 + J_2^2 + J_3^2}{4} - \frac{K_1^2 + K_2^2 + K_3^2}{16}, \\ B = & \frac{K_1K_2K_3}{32} \cos(2\kappa) \\ & - \frac{4J_1J_2J_3 + J_1K_1K_3 + J_2K_1K_2 + J_3K_2K_3}{16} \cos \kappa \\ & + \frac{J_1J_3K_3 + J_2J_3K_2 + J_1J_2K_1}{8}. \end{aligned} \quad (6)$$

The magnetic ground-state energy is $E_0 = \sum_{i=1}^p \sum'_{\kappa} \Lambda_{i,\kappa}$ where the prime means that the sum contains $\Lambda_{i,\kappa} < 0$ only. In the thermodynamic limit we get the following formula for the ground-state energy per site:

$$e_0 = - \sum_{i=1}^p \frac{1}{2p\pi} \int_{-\pi}^{\pi} d\kappa |\Lambda_{i,\kappa}| \theta(-\Lambda_{i,\kappa}), \quad (7)$$

where $\theta(x)$ is the Heaviside step function.

The magnetic Helmholtz free energy is $F = -(1/\beta) \sum_{i=1}^p \sum_{\kappa} \ln[1 + \exp(-\beta\Lambda_{i,\kappa})]$, where $\beta=1/T$ is the inverse temperature. The magnetic Helmholtz free energy per site in the thermodynamic limit is given by

$$f = - \frac{1}{\beta} \sum_{i=1}^p \frac{1}{2p\pi} \int_{-\pi}^{\pi} d\kappa \ln[1 + \exp(-\beta\Lambda_{i,\kappa})]. \quad (8)$$

In the zero-temperature limit $\beta \rightarrow \infty$ Eq. (8) transforms into Eq. (7) as it should.

Using the representation in terms of spinless fermions (4) we can calculate rigorously various quantities for the spin chain under consideration [see Eqs. (15), (16), and (18) below].

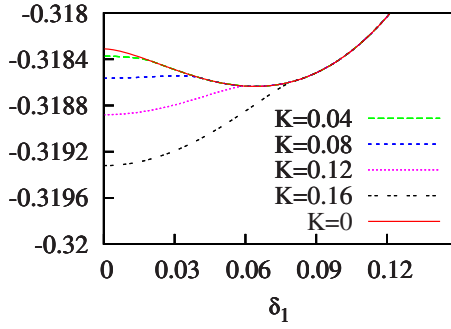


FIG. 1. (Color online) Total ground-state energy per site $\mathcal{E}(\delta_1)$ for dimerized system as K increases. $J=1$, $\alpha=0.5$, $K=0, 0.04, 0.08, 0.12, 0.16$ (from top to bottom).

III. PHASE DIAGRAMS

A. Case $T=0$

We start with the zero-temperature case. In our further analysis we fix the energy units putting $|J|=1$, assume without loss of generality $J>0$ and $K\geq 0$, and take $N=100\,000$ for $p=2$ and $N=100\,002$ for $p=3$. Next, we calculate ground-state energy (7) for dimerized system [i.e., with a distortion pattern $\delta_1\delta_2\delta_1\delta_2\dots$, $\delta_1+\delta_2=0$, see Eqs. (5) and (2)] and for trimerized system [i.e., with a distortion pattern $\delta_1\delta_2\delta_3\delta_1\delta_2\delta_3\dots$, $\delta_1+\delta_2+\delta_3=0$, see Eqs. (6) and (2)] varying K from 0 to 3 for fixed α (say $\alpha=0.5$) to get a general insight into the behavior of the total ground-state energy per site $\mathcal{E}(\{\delta_n\})$.

Some typical dependences of the total ground-state energy of the dimerized system on δ_1 as K deviates from zero and increases are shown in Fig. 1. Figure 2 shows the total ground-state energy per site $\mathcal{E}(\delta_1, \delta_2)$ for the trimerized case. The period-3 lattice distortions are parameterized by δ_1 and δ_2 ($\delta_1+\delta_2+\delta_3=0$). The panels of Fig. 2 correspond to the values $K, K=1.3, 1.9, 2.4, 3$, (top to bottom) of the three-site interaction. In the dimerized case the energy $\mathcal{E}(\delta_1)$ may exhibit one or more minima. That is also true for $\mathcal{E}(\delta_1, \delta_2)$ in the trimerized case, $p=3$. In that case, however it is sufficient to consider the line $\delta_1=\delta_2$. The reason for this is the invariance of the physics with respect to a renumbering of the sites in a period-3 chain. Due to that symmetry extremum points of $\mathcal{E}(\delta_1, \delta_2)$ can only lie along the three straight lines $\delta_1=\delta_2$, $\delta_1=-2\delta_2$, $\delta_1=-\delta_2/2$, and these lines are equivalent to each other.²³ For simplicity we denote $\mathcal{E}(\delta_1, \delta_2=\delta_1)$ for the trimerized system by $\mathcal{E}(\delta_1)$, as in the dimerized case. Typical dependences $\mathcal{E}(\delta_1)$ for the trimerized system for K around K_{crit} are shown in Fig. 3. Below we discuss the dependence $\mathcal{E}(\delta_1)$ for the cases $p=2$ and $p=3$ in more detail.

1. Dimerization

For the dimerized case, $\delta_1=-\delta_2$, the changes in the behavior of $\mathcal{E}(\delta_1)$ as K increases are quite simple. First, we note that due to symmetry $\mathcal{E}(\delta_1)=\mathcal{E}(-\delta_1)$, and we consider further only $\delta_1\geq 0$. We observe that $\mathcal{E}(\delta_1)$ shows one minimum at $\delta_1\neq 0$ if K does not exceed a certain value K_a ; two minima at $\delta_1=0$ and $\delta_1\neq 0$ occur for $K_a\leq K\leq K_c$; at a value $K=K_b$ within that interval the depths of the two minima become

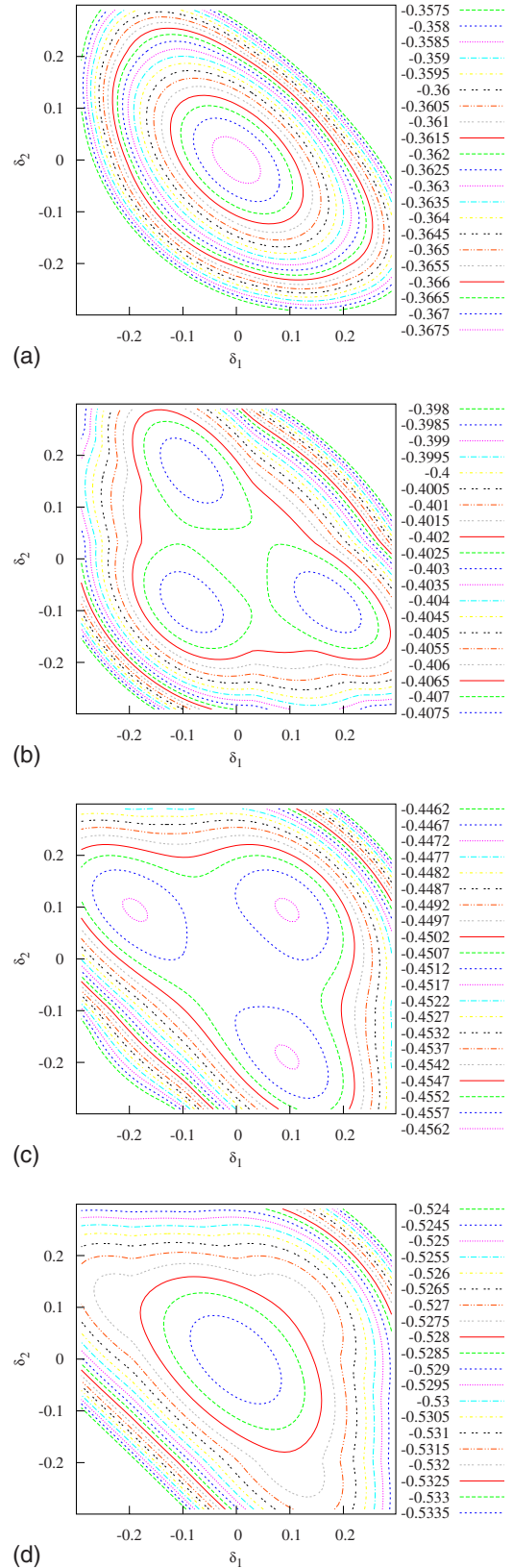


FIG. 2. (Color online) Total ground-state energy per site $\mathcal{E}(\delta_1, \delta_2)$ versus δ_1 and δ_2 for trimerized system (distortion pattern $\delta_1\delta_2\delta_3\delta_1\delta_2\delta_3\dots$, $\delta_1+\delta_2+\delta_3=0$) for $J=1$, $\alpha=0.5$, (a) $K=1.3$, (b) $K=1.9$, (c) $K=2.4$, (d) $K=3$. All minima are located along the lines $\delta_1=\delta_2$, $\delta_1=-2\delta_2$, $\delta_1=-\delta_2/2$.

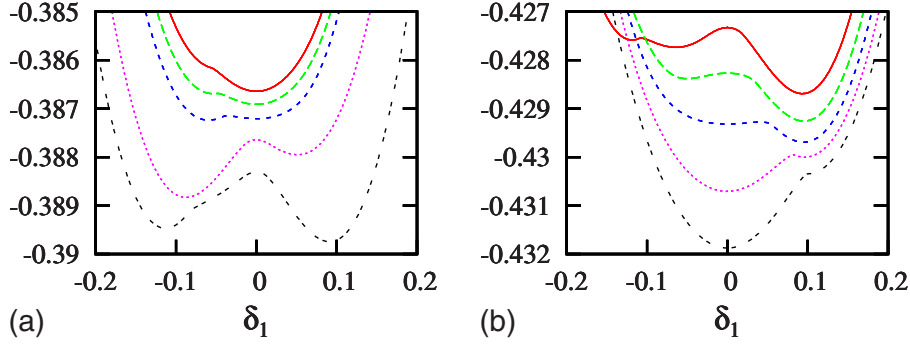


FIG. 3. (Color online) Total ground-state energy per site $\mathcal{E}(\delta_1)$ for trimerized system as K increases. $J=1$, $\alpha=0.5$, (a) $K = 1.6, 1.65, 1.7, 1.9, 2.1$ (from top to bottom), (b) $K=2.15, 2.3, 2.5, 2.8, 3$ (from top to bottom). Notice that for clarity the curves corresponding to $K=1.65, 1.7, 1.9, 2.1$ and $K=2.3, 2.5, 2.8, 3$ have been shifted upwards by $0.003, 0.006, 0.019,$ and 0.034 and $0.0155, 0.0385, 0.076,$ and 0.102 , respectively.

equal. For K exceeding K_c $\mathcal{E}(\delta_1)$ has only one minimum at $\delta_1=0$. This behavior, shown in Fig. 1, is typical for a (ground-state) phase transition of first order, where the phase-transition point is at $K=K_b$ and where $[K_a, K_c]$ is the interval in which metastable states occur. The value of δ_1 which yields the lowest energy (denoted further δ_1^*) plays the role of an order parameter. For $\alpha=0.5$ the order parameter $\delta_1^*(K)$ is shown in Fig. 4(a) (open-circle line). Also shown there are the stationary points $\tilde{\delta}_1$ where $\partial\mathcal{E}(\delta_1)/\partial\delta_1=0$. There are always either two (as for $K \leq K_a$), or three ($K_a < K < K_c$), or one ($K_c < K$) stationary point present. In the case of three stationary points, the two outer ones are minima (the stable and metastable states of the system, thick solid lines), with a maximum (thin dash-dot line) between them. From the data shown in Fig. 4(a) we find $K_a \approx 0.0645$ and $K_c \approx 0.125$ for the limits of the metastable region and $K_b \approx 0.0905$ for the phase-transition point, where the order parameter jumps from $\delta_1^* \approx 0.064$ to zero. These K values are marked by bold dots in Fig. 4.

The order parameter $\delta_1^*(K < K_b) > 0$ in Fig. 4(a) is obviously constant. That fact may be explained as follows. The numerical data from Fig. 1 show that the K -dependent contribution to the ground-state energy vanishes for δ_1 larger than some K -dependent threshold value. That explains why the minimum of $\mathcal{E}(\delta_1)$ stays fixed as long as K is small enough. This behavior of $\mathcal{E}(\delta_1)$ can be understood by taking another look at dispersion (5) for the situation at hand, $J_1 = 1 - \delta_1$, $J_2 = 1 + \delta_1$, $K_1 = K_2 = K$. We then have

$$\Lambda_{i,\kappa} = -\frac{K}{2} \cos \kappa \pm \frac{1}{\sqrt{2}} \sqrt{1 + \cos \kappa + \delta_1^2 (1 - \cos \kappa)}, \quad (9)$$

and at the Brillouin-zone boundaries, $\kappa = \pm \pi$, we have $\Lambda_{1,\pm\pi} = (K/2) - |\delta_1|$ and $\Lambda_{2,\pm\pi} = (K/2) + |\delta_1|$. That means that for $K < 2|\delta_1|$ the lower band is completely “submerged” ($\Lambda_{1,\kappa} < 0$) while for the upper band $\Lambda_{2,\kappa} > 0$. [We note that the gapped excitations for $K < |J_1 - J_2|$ were reported in Ref. 24, compare the discussion around Eq. (12) of that paper.] The ground-state energy then is given by the sum of *all* $\Lambda_{i,\kappa}$ and hence the K -dependent contribution vanishes, being a sum over $\cos \kappa$, see Eq. (9). For smaller values of δ_1 (or larger values of K) the lower band crosses the zero level and

the ground-state energy becomes K dependent.

Repeating the calculations reported in Fig. 4(a) for various α we construct the ground-state phase diagram in the plane $K-\alpha$, Fig. 4(b), demonstrating how increasing K first

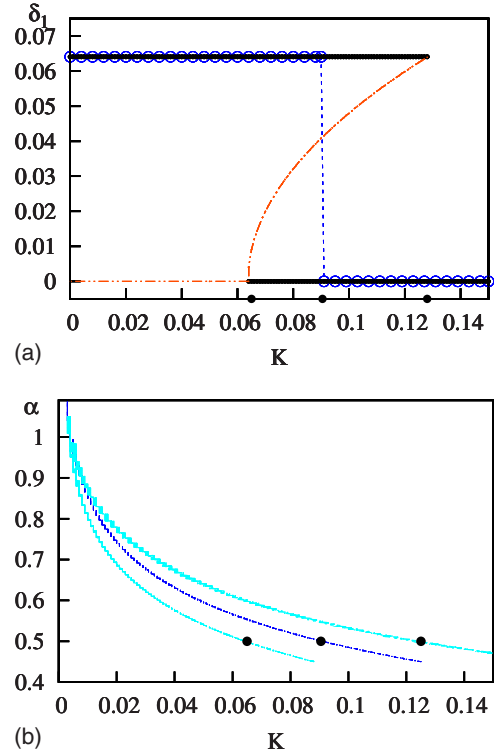


FIG. 4. (Color online) Order parameter and ground-state phase diagram for dimerized chain, $J=1$. (a) Order parameter $\delta_1^*(K)$ (open circles) and stationary points $\tilde{\delta}_1(K)$ of the total ground-state energy per site $\mathcal{E}(\delta_1)$ [thick solid lines (minima) and thin dash-dot lines (maxima)], $\alpha=0.5$. Note that the horizontal open-circle lines for the order parameter coincide with the thick solid lines indicating the deeper minimum of $\mathcal{E}(\delta_1)$. (b) Ground-state phase diagram in the plane $K-\alpha$. The left light (cyan) curve corresponds to $K_a(\alpha)$, the middle dark (blue) curve corresponds to $K_b(\alpha)$, the right light (cyan) curve corresponds to $K_c(\alpha)$, where K_a and K_c are the limits of the metastable region and K_b is the phase-transition point. In both panels we also denote the values of K_a , K_b , and K_c (from left to right) for $\alpha=0.5$ by bold dots.

makes the dimerized state metastable and then completely suppresses it in favor of the uniform state.

2. Trimerization

We move to the trimerization patterns which emerge near $K=K_{\text{crit}}$. The changes in $\mathcal{E}(\delta_1)$ as K increases are more complicated than in the dimerized case (see Fig. 3). First, in addition to the minimum at $\delta_1=0$, when K surpasses K_d , a minimum at $\delta_1<0$ (the corresponding bond pattern is “strong bond–strong bond–weak bond”) appears, which, when K exceeds $K_e>K_d$, becomes the lowest-energy one. With further increase in K , when K surpasses K_f , another minimum at $\delta_1>0$ (the corresponding bond pattern is “weak bond–weak bond–strong bond”) appears, which, when K exceeds $K_g>K_f$, becomes the lowest-energy one. Then, as K exceeds K_h , the dependence $\mathcal{E}(\delta_1)$ exhibits three minima, two of which occur for $\delta_1<0$ and the deepest one at $\delta_1>0$ [see the solid (red) curve corresponding to $K=2.15$ in Fig. 3(b)]. With further increase in K , as K exceeds K_i , the dependence $\mathcal{E}(\delta_1)$ shows only two minima: for $\delta_1<0$ and the deeper one for $\delta_1>0$. As K becomes larger than $K_j>K_i$ the two minima are located at $\delta_1=0$ and (the deeper one) at $\delta_1>0$. At $K=K_k$ the depth of these minima is the same. Finally, for $K>K_l$ the minimum at $\delta_1>0$ disappears and the uniform pattern with $\delta_1=0$ becomes favorable. The behavior of the order parameter $\delta_1^*(K)$ described above, together with a set of stationary points $\tilde{\delta}_1(K)$ for $\alpha=0.5$, is shown in Fig. 5(a). The specific values of the three-site coupling for that example are as follows: $K_d \approx 1.633$, $K_e \approx 1.693$, $K_f \approx 1.745$, $K_g \approx 2.080$, $K_h \approx 2.130$, $K_i \approx 2.175$, $K_j \approx 2.418$, $K_k \approx 2.610$, $K_l \approx 2.999$.

Repeated calculations of $\delta_1^*(K)$ and $\tilde{\delta}_1(K)$ for various α yield a phase diagram [see Fig. 5(b)]. We show by dark (blue) curves $K_e(\alpha)$, $K_g(\alpha)$, and $K_k(\alpha)$ which correspond to ground-state phase transitions of first order. Light (cyan) curves $K_d(\alpha)$, $K_f(\alpha)$, $K_h(\alpha)$, $K_i(\alpha)$, $K_j(\alpha)$, and $K_l(\alpha)$ indicate the regions of metastability.

3. Analytical arguments for trimerization

As can be seen from Fig. 5(b) the phase diagram becomes extremely simple in the limit $K=K_{\text{crit}}$, $\alpha \rightarrow \infty$, indicating a possible simplification of the analysis for that case. More detailed consideration confirms this expectation. In fact, for the trimerized system with $K=2J$ and small (but nonzero) δ_1 (i.e., for a stiff lattice having large elastic constant α) the magnetic ground-state energy per site [Eq. (7)] reads

$$e_0(\delta_1) = \frac{1}{6\pi} \int_{-\pi}^{\pi} d\kappa \Lambda_{1,\kappa}, \quad (10)$$

where the energy of the lowest-energy band $\Lambda_{1,\kappa}<0$ can be written in the form $\Lambda_{1,\kappa}/J=M_1(\kappa)M_2(\kappa)$. Here $M_2(\kappa)$ for $\delta_1 \rightarrow 0$ is an almost constant function for $-\pi \leq \kappa < \pi$, with values close to 1 and

$$\begin{aligned} M_1(\kappa) &= -\sqrt{2\sqrt{1+(1+\aleph^2)\delta_1^2} + (-1+2\aleph\delta_1^2)\cos\kappa} \\ &= -\sqrt{2\sqrt{2+(1-\aleph^2)\delta_1^2}} \sqrt{1-z^2 \cos^2 \frac{\kappa}{2}}, \end{aligned}$$

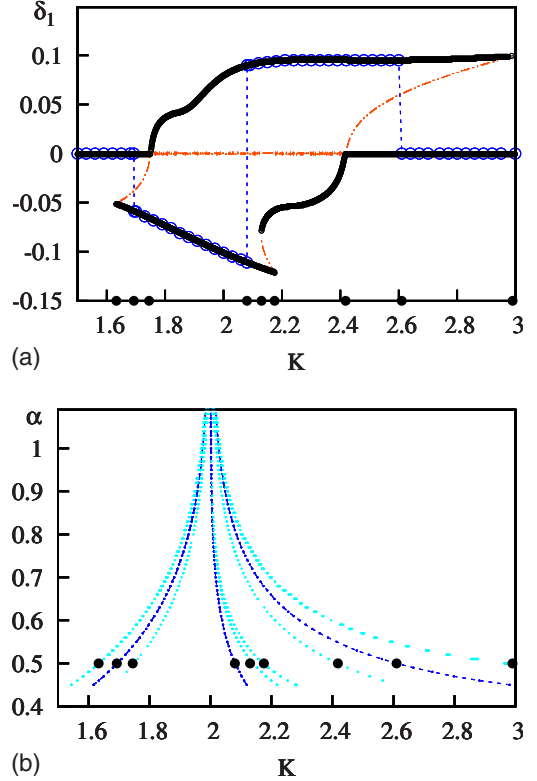


FIG. 5. (Color online) Order parameter and ground-state phase diagram for trimerized chain, $J=1$. (a) Order parameter $\delta_1^*(K)$ (open circles) and stationary points $\tilde{\delta}_1(K)$ of the total ground-state energy per site $\mathcal{E}(\delta_1)$ [thick solid lines (minima) and thin dash-dot lines (maxima)], $\alpha=0.5$. (b) Ground-state phase diagram in the plane $K-\alpha$. From left to right the curves correspond to $K_d(\alpha)$ [light (cyan)], $K_e(\alpha)$ [dark (blue)], $K_f(\alpha)$ [light (cyan)], $K_g(\alpha)$ [dark (blue)], $K_h(\alpha)$ [light (cyan)], $K_i(\alpha)$ [light (cyan)], $K_j(\alpha)$ [light (cyan)], $K_k(\alpha)$ [dark (blue)], $K_l(\alpha)$ [light (cyan)]. The dark (blue) curves are first-order ground-state phase transitions, the light (cyan) curves denote limits of metastability, i.e., points where minima in the total ground-state energy appear or disappear (compare Fig. 3). In both panels we also denote the values of K_d, \dots, K_l (from left to right) for $\alpha=0.5$ by bold dots.

$$z^2 = \frac{2(1-2\aleph\delta_1^2)}{2+(1-\aleph^2)\delta_1^2},$$

$$(z')^2 \equiv 1-z^2 = \frac{(1+\aleph)^2}{2+(1-\aleph^2)\delta_1^2} \delta_1^2 \approx \frac{(1+\aleph)^2}{2} \delta_1^2. \quad (11)$$

$M_1(\kappa)$ and $M_2(\kappa)$ result from the trigonometric solution of the cubic equation for $\Lambda_{i,\kappa}$, discussed in Sec. II. Neglecting the factor $M_2(\kappa) \lesssim 1$ and using Eq. (11) ground-state energy (10) becomes

$$e_0(\delta_1) \approx -\frac{2\sqrt{2}}{3\pi} \sqrt{2+(1-\aleph^2)\delta_1^2} E(z)J, \quad (12)$$

where $E(z) \equiv \int_0^{\pi/2} d\varphi \sqrt{1-z^2 \sin^2 \varphi}$ is the complete elliptical integral of the second kind. For $z^2 \approx 1$, hence $(z')^2 \equiv 1-z^2 \ll 1$ we have²⁵

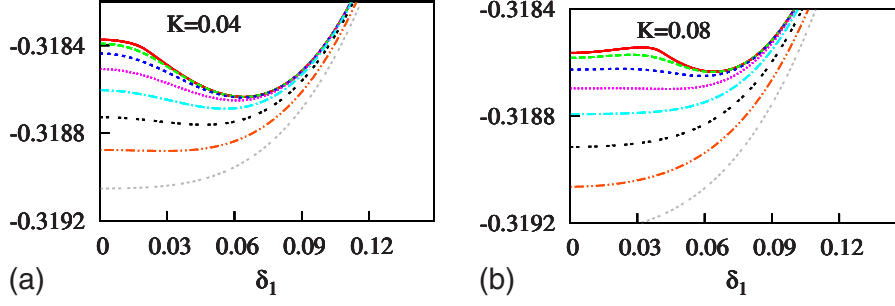


FIG. 6. (Color online) Total Helmholtz free energy per site $\mathcal{F}(\delta_1)$ for dimerized system with $J=1$, $\alpha=0.5$, (a) $K=0.04$, and (b) $K=0.08$ as temperature increases, $T=0.001, 0.006, 0.011, 0.016, 0.021, 0.026, 0.031, 0.036$ (from top to bottom).

$$E(z) = 1 + \frac{1}{2} \left(\Lambda - \frac{1}{2} \right) (z')^2 + \frac{3}{16} \left(\Lambda - \frac{13}{12} \right) (z')^4 + \frac{15}{128} \left(\Lambda - \frac{6}{5} \right) \times (z')^6 + \dots, \quad \Lambda \equiv \ln \frac{4}{z'}. \quad (13)$$

Using the first two terms on the right-hand side of Eq. (13) to write the total ground-state energy per site of the trimerized system $\mathcal{E}(\delta_1) = e_0(\delta_1) + 2\alpha\delta_1^2$ and minimizing $\mathcal{E}(\delta_1)$ with respect to δ_1 we get

$$|\delta_1^*| = \exp\left(a - b\frac{\alpha}{J}\right) > 0, \quad (14)$$

where a and $b > 0$ are some coefficients, the precise values of which are not important here. Equation (14) explicitly demonstrates the instability. The simple reason for the trimerization at $K=K_{\text{crit}}$ is the $\delta_1^2 \ln \delta_1$ term in the small- δ_1 expansion of the magnetic ground-state energy $e_0(\delta_1)$, similar to the dimerized case.¹³

Two more remarks are in order here. First, we notice that

although omitting $M_2(\kappa) \lesssim 1$ has no influence on the *existence* of a nonzero value of the trimerization parameter δ_1^* , the actual value of that parameter is sensitive to the approximation made since we slightly overestimate the value of the magnetic part of the total ground-state energy. Second, from Fig. 5(b) we also notice that for $K=2$ the spin system exhibits two energy minima, and the one which corresponds to $\delta_1 < 0$ is deeper. Obviously, the approximate total ground-state energy based on Eq. (12) depends only on δ_1^2 and thus cannot reproduce this fine feature.

B. Case $T > 0$

We turn to the finite-temperature case. Now we must calculate magnetic Helmholtz free energy (8) for dimerized and trimerized systems and examine the total Helmholtz free energy per site $\mathcal{F}(\delta_1)$. Some typical profiles for $\mathcal{F}(\delta_1)$ are shown in Fig. 6 (dimerized systems) and in Fig. 7 (trimerized systems). We find that as temperature starts to increase the ground-state picture for lattice distortion patterns may change significantly. Thus, the first-order phase transition

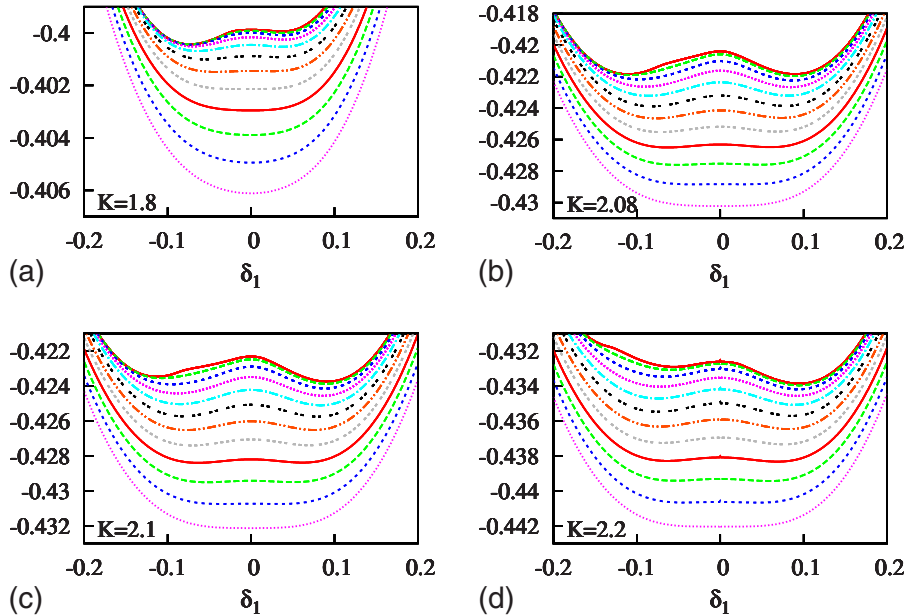


FIG. 7. (Color online) Total Helmholtz free energy per site $\mathcal{F}(\delta_1)$ for trimerized system with $J=1$, $\alpha=0.5$, (a) $K=1.8$, (b) $K=2.08$, (c) $K=2.1$, (d) $K=2.2$ as temperature increases, $T=0.002, 0.012, 0.022, 0.032, 0.042, 0.052, 0.062, 0.072, 0.082, 0.092, 0.102, 0.112$ (from top to bottom).

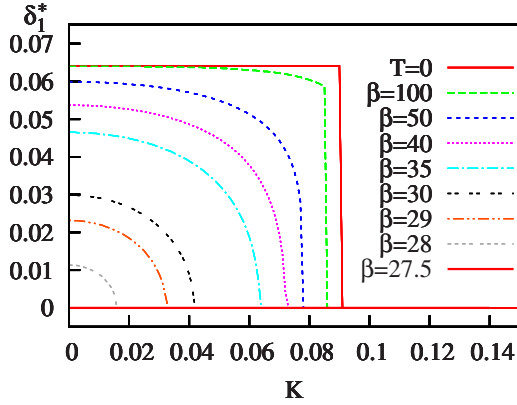


FIG. 8. (Color online) Dimerization order parameter δ_1^* versus K as temperature increases, $J=1$, $\alpha=0.5$. $\beta=\infty, 100, 50, 40, 35, 30, 29, 28, 27.5$ [from top (or from right) to bottom (or to left)]. For $\beta=27.5$ we have already $\delta_1^*=0$ for all K (horizontal line $\delta_1^*=0$).

from dimerized to uniform phase tuned by increasing K may become of second-order as temperature increases, and for sufficiently high temperatures may completely disappear (see Fig. 8). Temperature effects are even more drastic for lattice trimerization (see Fig. 9). The first-order phase transitions between uniform and trimerized phases at K_e and K_k may become of second order. The phase transition between two different trimerized patterns at K_g remains of first order as temperature increases (see Fig. 9), however, for higher temperatures the trimerized phase with $\delta_1^* < 0$ does not appear and the system shows the trimerized lattice pattern “weak bond–weak bond–strong bond” only as K enters a corresponding region (see the curve for $\beta=8.75$ in Fig. 9). Finally, for sufficiently high temperatures (as for $\beta=8.5$ in Fig. 9) trimerization does not occur at all.

Another way to discuss finite-temperature effects is to follow the temperature dependence of the order parameter δ_1^* for different K (Figs. 10 and 11). For small K the temperature dependence of the dimerization parameter corresponds to the scenario of a second-order phase transition driven by temperature that agrees with the known results in the limit $K=0$.¹³ For larger values of K the dimerization order parameter abruptly becomes zero above a certain temperature. Moreover, for K approaching K_b the dimerization order parameter immediately vanishes as temperature deviates from zero. The details of that behavior are displayed in Fig. 10. We note here that the two-site next-nearest-neighbor exchange interaction effect on the spin-Peierls critical temperature was discussed earlier in Ref. 19. Within the approximate approach elaborated in that paper the authors found that the spin-Peierls temperature may either increase or decrease depending on the sign of the next-nearest-neighbor coupling J_2 . Namely, the spin-Peierls temperature increases (decreases) if J_2 is antiferromagnetic (ferromagnetic). In contrast, the spin-Peierls temperature does not depend on the sign of the three-site coupling K , although the three-site interactions noticeably affect the appearance of the spin-Peierls phase at low temperature.

The temperature dependence of the trimerization order parameter for different K is even more intriguing. Thus, as K exceeds K_e the trimerized phase characterized by $\delta_1^* < 0$

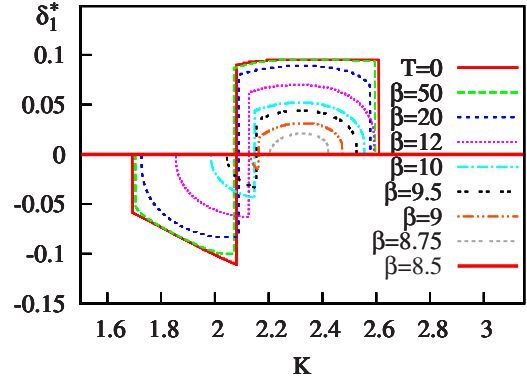


FIG. 9. (Color online) Trimerization order parameter δ_1^* versus K as temperature increases, $J=1$, $\alpha=0.5$. $\beta=\infty, 50, 20, 12, 10, 9.5, 9, 8.75, 8.5$ (as β increases the dependence δ_1^* versus K approaches the line $\delta_1^*=0$). For $\beta=8.5$ we have already $\delta_1^*=0$ for all K .

emerges in the ground state. With increasing temperature the order parameter $\delta_1^* < 0$ vanishes either discontinuously or continuously [see Fig. 11(a) and also Fig. 7(a)]. However, when K is around K_g with increasing temperature two minima of the total Helmholtz free energy at negative and positive δ_1 compete with each other [see Fig. 7(b)] producing the behavior of the order parameter shown by the solid (red) line in Fig. 11(b) ($K=2.08$). For larger values of K the ground-state trimerized pattern is characterized by $\delta_1^* > 0$; with increasing temperature the order parameter $\delta_1^* > 0$ vanishes either continuously or discontinuously [see Fig. 11(c) and also Fig. 7(d)]. Even more complicated behavior, as for $K=2.58$ [long-dashed (green) curve in Fig. 11(c)], may also emerge.

To summarize this section, the ground-state lattice instabilities owing to the spin-Peierls mechanism survive at low temperatures, but their behavior changes as temperature increases. Different ground-state phases may disappear at different temperatures, but ultimately all instabilities are destroyed by thermal fluctuations as temperature becomes sufficiently high. It is worth noticing that the characteristic temperatures for dimerization and trimerization might be different (as in Figs. 10 and 11; note that these data correspond

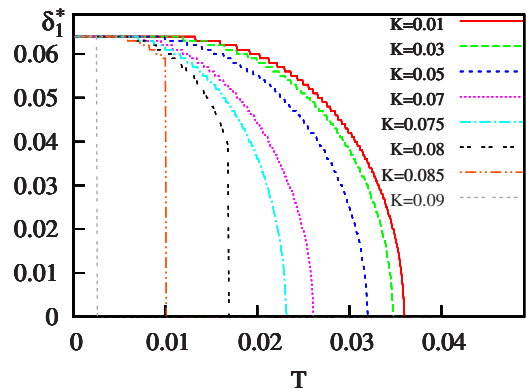


FIG. 10. (Color online) Dimerization order parameter δ_1^* versus temperature as K increases, $J=1$, $\alpha=0.5$. $K=0.01, 0.03, 0.05, 0.07, 0.075, 0.08, 0.085, 0.09$ [from top (or from right) to bottom (or to left)].

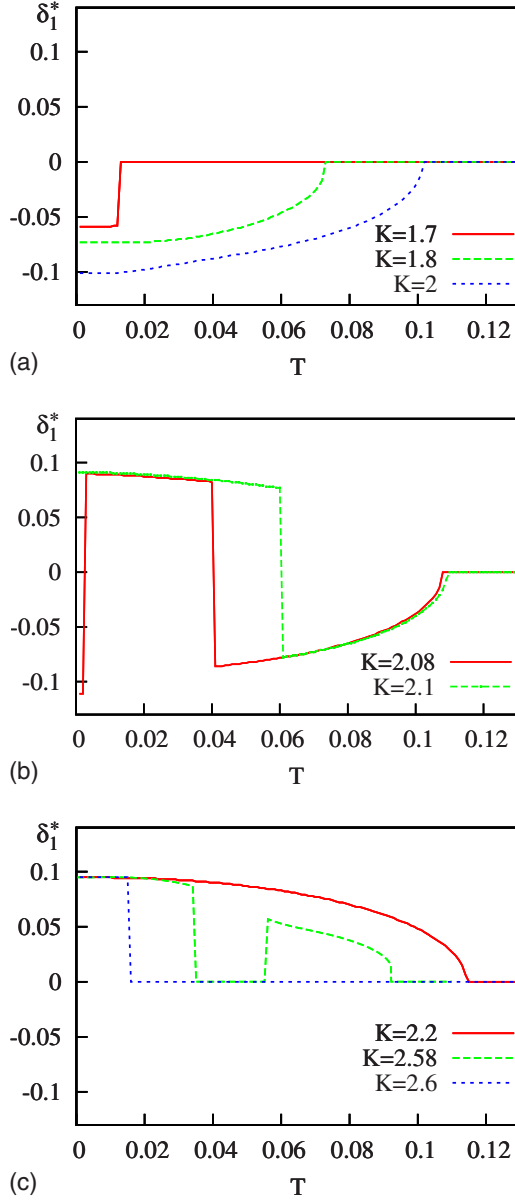


FIG. 11. (Color online) Trimerization order parameter δ_1^* versus temperature as K increases, $J=1$, $\alpha=0.5$. (a) $K=1.7$ [solid (red)], $K=1.8$ [long-dashed (green)], $K=2$ [short-dashed (blue)]; (b) $K=2.08$ [solid (red)], $K=2.1$ [long-dashed (green)]; (c) $K=2.2$ [solid (red)], $K=2.58$ [long-dashed (green)], $K=2.6$ [short-dashed (blue)].

to $\aleph=1$; at the same time one should bear in mind that the typical interaction energy scales for dimerization, $J=1$, $K \approx 0$, and trimerization, $J=1$, $K \approx 2$, are different).

IV. GROUND-STATE AND FINITE-TEMPERATURE PROPERTIES

The ground-state and finite-temperature properties of spin chain (1) have been discussed in some detail in previous studies. In particular, the role of the three-site interactions controlled by K has been illustrated for both static¹⁰ and dynamic²⁶ properties of the spin model. (We also note that some static properties of a structurally dimerized spin chain

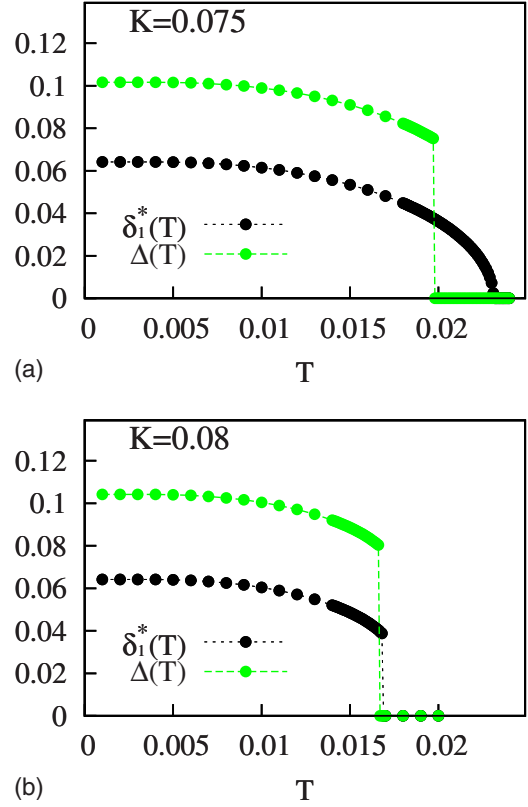


FIG. 12. (Color online) Energy gap $\Delta(T)$ [light (green) symbols] and dimerization order parameter $\delta_1^*(T)$ [dark (black) symbols] versus temperature T ($J=1$, $\alpha=0.5$). (a) $K=0.075$; (b) $K=0.08$.

with interactions J_1 , J_2 , and K have been discussed in Ref. 24; those findings are relevant for the deformable spin chain in question here, if for the given set of parameters the dimerized phase is energetically most favorable.) Now we allow for lattice deformations within spin chain (1) and discuss the static properties of such a system at $T=0$ and $T>0$. The phase diagrams obtained in Sec. III show which specific lattice deformation pattern is adopted by the system for a concrete set of parameters (i.e., values of K and T , since we fixed $J=1$, $\aleph=1$, and $\alpha=0.5$). It must be kept in mind that only a limited set of possible lattice configurations has been taken into consideration. Nevertheless it can be said with certainty that for $K \leq K_b$ or $K_e \leq K \leq K_\kappa$ the uniform lattice is unstable with respect to dimerization or trimerization, respectively, and hence the properties of the system will definitely differ from those of the uniform lattice.

We begin with the energy gap. To find the energy gap $\Delta(T)$ we evaluate the elementary excitation energies $\Lambda_{i,\kappa}$ [see Eqs. (4)–(6)] in terms of the order parameter $\delta_1^*(T)$ [we use the results of Sec. III for $\delta_1^*(T)$ as inputs for these calculations]. We denote the evaluated elementary excitation energies by $\Lambda_{i,\kappa}(T)$. The magnetic ground-state energy at a temperature T is given by $E_0(T) = \sum_{i=1}^p \sum_{\kappa} \Lambda_{i,\kappa}(T)$ [we recall that the prime means that the sum contains $\Lambda_{i,\kappa}(T) < 0$ only]. The energy gap $\Delta(T)$ is given by the energy of the first-excited state, i.e., the smallest value of $\Lambda_{i,\kappa}(T) \geq 0$. For the conventional XX chain (i.e., $K=0$) we have $\Delta(T=0) = |\delta_1^*(T=0)|J$ [see Eq. (9) (with $K=0$) and discussion just below it], and hence the energy gap is simply proportional to the dimeriza-

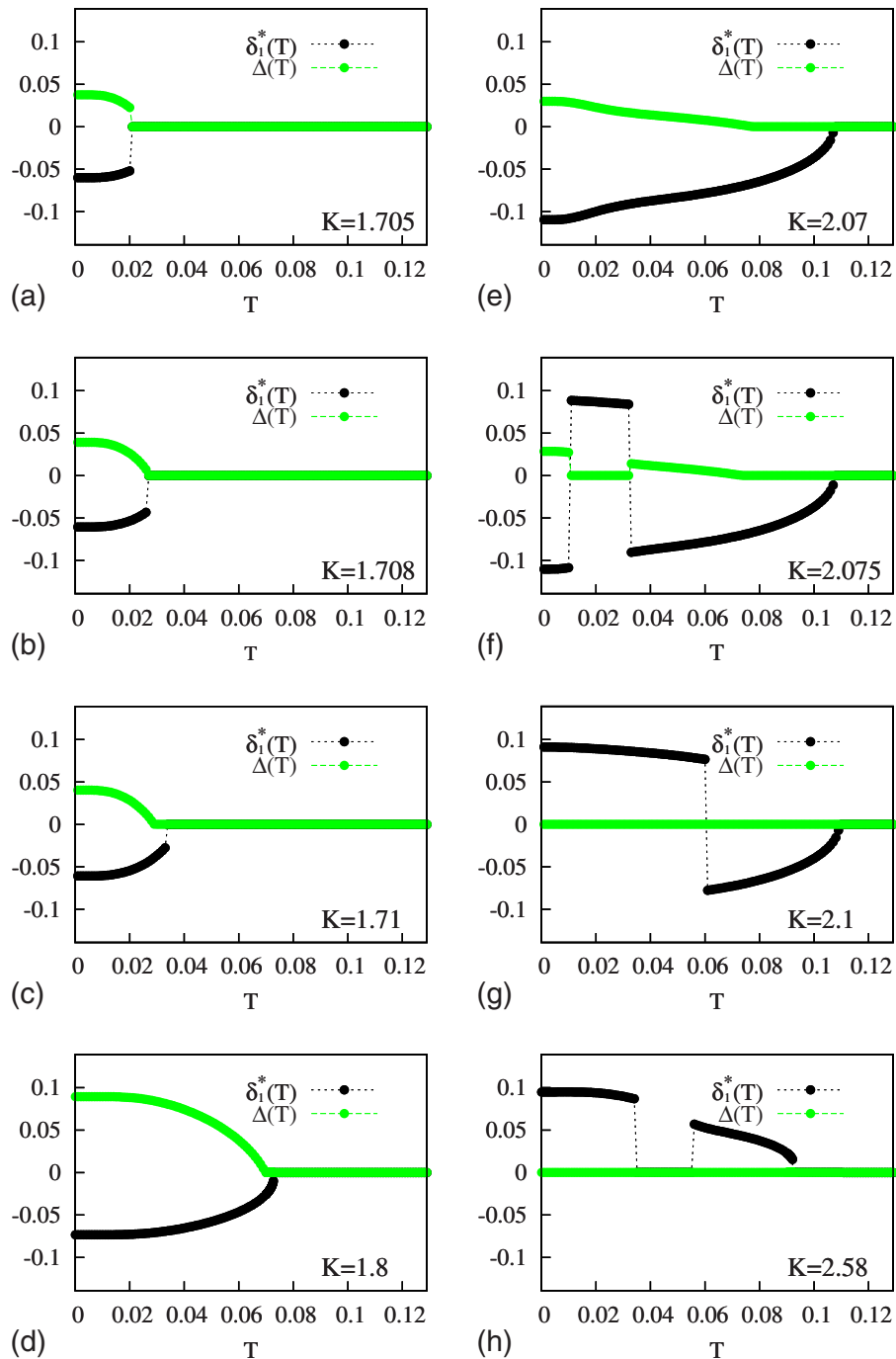


FIG. 13. (Color online) Energy gap $\Delta(T)$ [light (green) symbols] and trimerization order parameter $\delta_1^*(T)$ [dark (black) symbols] versus temperature T ($J=1, \alpha=0.5$). (a) $K=1.705$; (b) $K=1.708$; (c) $K=1.71$; (d) $K=1.8$; (e) $K=2.07$; (f) $K=2.075$; (g) $K=2.1$; (h) $K=2.58$.

tion parameter. However for $K > 0$ the relation between these two quantities may be more intricate. In Figs. 12 and 13 we report the results for the temperature-dependent energy gap $\Delta(T)$ [light (green) symbols] for small values K (when dimerization occurs) and for values of K around K_{crit} (when trimerization occurs), respectively. We also show the corresponding dependences of $\delta_1^*(T)$ for comparison. From these figures it is nicely seen that as temperature decreases the energy gap may open either continuously [as e.g., in Figs. 13(b)–13(d), etc.] or discontinuously [as e.g., in Fig. 12(a)]. The deformable spin chain may be dimerized but gapless

[e.g., slightly above $T=0.02$ in Fig. 12(a)] or dimerized and gapped [e.g., at low temperatures in Fig. 12(a)]. Interestingly, the deformable spin system may exhibit different trimerized patterns while remaining gapless [see Figs. 13(g) and 13(h)] or may show a trimerized pattern while simultaneously becoming gapless [see the temperatures around $T=0.02$ in Fig. 13(f)]. From the results reported in Figs. 12 and 13 it should be clear that the relation between the energy gap and the parameter characterizing a lattice distortion may be rather involved especially in the region where trimerized patterns come into being.

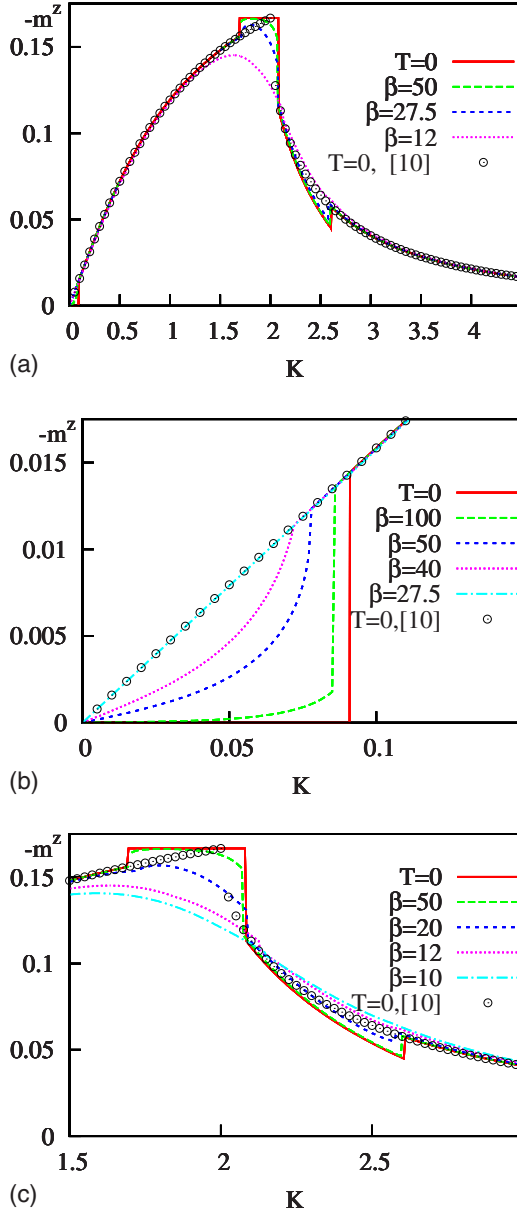


FIG. 14. (Color online) Transverse magnetization $-m^z$ versus K for the deformable spin chain ($J=1, \alpha=0.5$) for various temperatures. (a) $\beta=\infty, 50, 27.5, 12$; (b) $\beta=\infty, 100, 50, 40, 27.5$; (c) $\beta=\infty, 50, 20, 12, 10$. The results of panel (a) can be seen on a magnified scale in panels (b) and (c). The zero-temperature result for spin chain (1) obtained in Ref. 10 is shown by open circles.

We turn now to the transverse magnetization per site $m^z = \sum_{n=1}^N \langle s_n^z \rangle / N$, where $\langle (\dots) \rangle = \text{Tr}[\exp(-\beta H)(\dots)] / \text{Tr} \exp(-\beta H)$. In order to calculate m^z we introduce in Eq. (1) the additional term $-h \sum_{n=1}^N s_n^z$, where h is an infinitesimally small external magnetic field, evaluate $m^z = -\partial f / \partial h$, and then set $h=0$. As a result we get

$$m^z = -\frac{1}{2} \sum_{i=1}^p \frac{1}{2p\pi} \int_{-\pi}^{\pi} d\kappa \tanh \frac{\beta \Lambda_{i,\kappa}}{2}. \quad (15)$$

As it was noted in Refs. 9 and 10 spin model (1) exhibits a nonzero transverse magnetization $m^z \neq 0$ owing to the three-

site interactions of (XZX+YZY) type although there is no transverse field present in the model. The zero-temperature dependence m^z versus K for model (1) is shown by open circles in Fig. 14. The transition point at $K=K_{\text{crit}}$ is clearly indicated by the behavior of $m^z(K)$, the value of which shows a cusp-type maximum at $K=K_{\text{crit}}$, achieving the value 1/6 and monotonically decreases to zero as K goes to zero or to infinity.

If lattice distortions are allowed, $m^z(K)$ shows changes which are especially clearly visible at low temperatures (Fig. 14). First, for small K and low temperature the chain is dimerized and the transverse magnetization is reduced [Fig. 14(b)]. (See Fig. 8 for the K range of dimerization at a given temperature.) Deviations from the rigid-lattice results of Ref. 10 can also occur through trimerization, which is mainly observed (see Fig. 9) in the vicinity of $K=K_{\text{crit}}$. The non-monotonic changes in the transverse magnetization caused by the transition to trimerization are displayed in Fig. 14(c). As expected, the magnetization curves show sharper features at lower temperatures.

Next we discuss the static transverse susceptibility per site $\chi^z = \partial m^z / \partial h|_{h=0}$, which can be calculated according to the formula

$$\chi^z = \frac{\beta}{4} \sum_{i=1}^p \frac{1}{2p\pi} \int_{-\pi}^{\pi} d\kappa \frac{1}{\cosh^2 \frac{\beta \Lambda_{i,\kappa}}{2}}. \quad (16)$$

The zero-temperature value of the static transverse susceptibility $\chi^z(T=0)$ can be easily obtained by using the limit representation of the Dirac delta function $\delta(x) = \lim_{T \rightarrow 0} 1/[2T \cosh^2(x/T)]$. Now we may rewrite Eq. (16) for the limiting value at $T=0$ in the form

$$\chi^z(T=0) = \frac{1}{2} \sum_{i=1}^p \frac{1}{2p\pi} \int_{-\pi}^{\pi} d\kappa \delta\left(\frac{\Lambda_{i,\kappa}}{2}\right). \quad (17)$$

For the uniform chain ($p=1$) with $K=0$ we have to substitute $\Lambda_{i,\kappa} \rightarrow J \cos \kappa$, and therefore $\int_{-\pi}^{\pi} d\kappa \delta(\Lambda_{i,\kappa}/2) \rightarrow 4/|J|$ and, as a result, we arrive at the familiar result $\chi^z(T=0) = 1/(\pi|J|)$. For the uniform chain with $K \neq 0$ we have $\Lambda_{i,\kappa} \rightarrow J \cos \kappa - (K/2) \cos(2\kappa)$, and hence $\chi^z(T=0) \rightarrow \infty$ for $K=K_{\text{crit}}$. Moreover, we can easily understand why χ^z is zero at $T=0$ in the dimerized phase of the conventional XX chain:¹³ The simple reason for that is that $\Lambda_{i,\kappa} \neq 0$ for all κ . In the presence of the three-site couplings the elementary excitation energies $\Lambda_{i,\kappa}$ become complicated functions of κ . However, $\chi^z(T=0) \neq 0$ until there exist κ for which $\Lambda_{i,\kappa}=0$. Thus, a nonzero value of χ^z at $T=0$ immediately signalizes that the energy gap (at $T=0$) is zero and vice versa, a zero value of $\chi^z(T=0)$ means that $\Delta(T=0) \neq 0$. This can be nicely seen in Fig. 15 where we show the temperature dependence of χ^z for different values of K [compare the $T \rightarrow 0$ results for small K in Fig. 15(a) and for $K=1.8, 2.08$ in Fig. 15(b) (gapped case) with the $T \rightarrow 0$ results for $K=2.1, 2.2$ in Fig. 15(b) (gapless case)]. The temperature dependences of χ^z shown in Fig. 15 correlate with the changes in lattice structure indicated by δ_1^* in Figs. 10 and 11.

Finally we discuss the specific heat per site $c = -T \partial^2 f / \partial T^2$ which can be calculated according to the formula

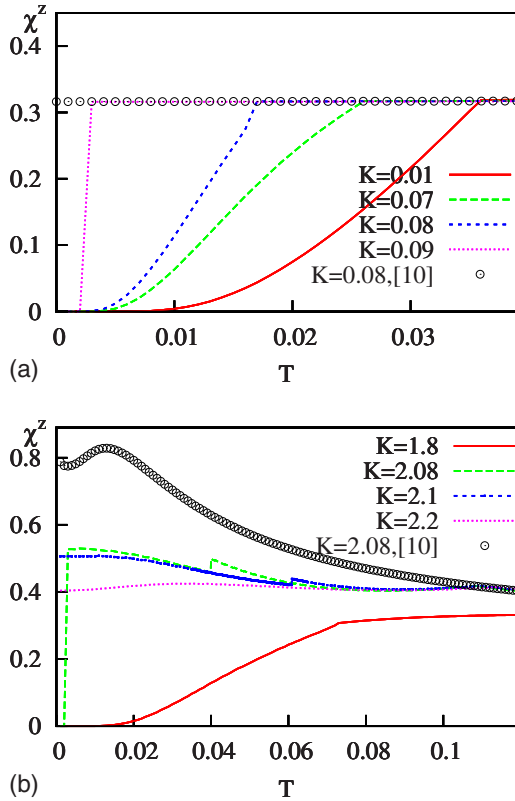


FIG. 15. (Color online) Temperature dependence of the static transverse susceptibility χ^z for the deformable spin chain ($J=1, \alpha=0.5$) for various values of K . (a) $K=0.01, 0.07, 0.08, 0.09$; (b) $K=1.8, 2.08, 2.1, 2.2$. We also show the results for rigid spin chain (1) with $J=1, K=0.08$, and $K=2.08$ as they follow from Ref. 10 (open circles).

$$c = \sum_{i=1}^p \frac{1}{2p\pi} \int_{-\pi}^{\pi} d\kappa \left(\frac{\frac{\beta\Lambda_{i,K}}{2}}{\cosh \frac{\beta\Lambda_{i,K}}{2}} \right)^2. \quad (18)$$

We recall from Ref. 10 that the ground-state phase transition inherent in model (1) produces anomalous low-temperature behavior in the vicinity of $K=K_{\text{crit}}$. Most clearly this anomaly is seen in the low-temperature behavior of the specific heat c . Away from the critical point $c \propto T$ at low temperatures [open circles in Fig. 16(a)], however, in the vicinity of the critical point c exhibits an anomalous square-root dependence on T at low temperatures, $c \propto \sqrt{T}$. The crossover from linear to square-root behavior can be seen in the data for $K=2.08 > K_{\text{crit}}=2$ (open circles) in Fig. 16(b).

If allowance is made for an elastic distortion of the lattice, the temperature dependence of the specific heat in the low-temperature region may be different from the rigid-lattice predictions (in the high-temperature region the lattice is not distorted and the temperature dependence of the specific heat is the same as for the uniform lattice). For small K , when the lattice is dimerized at low temperatures but is uniform for higher temperatures, the specific heat exhibits a behavior as in Fig. 16(a), whereas for K around K_{crit} , when trimerized patterns may emerge at low temperatures, the specific heat exhibits a behavior as in Fig. 16(b).

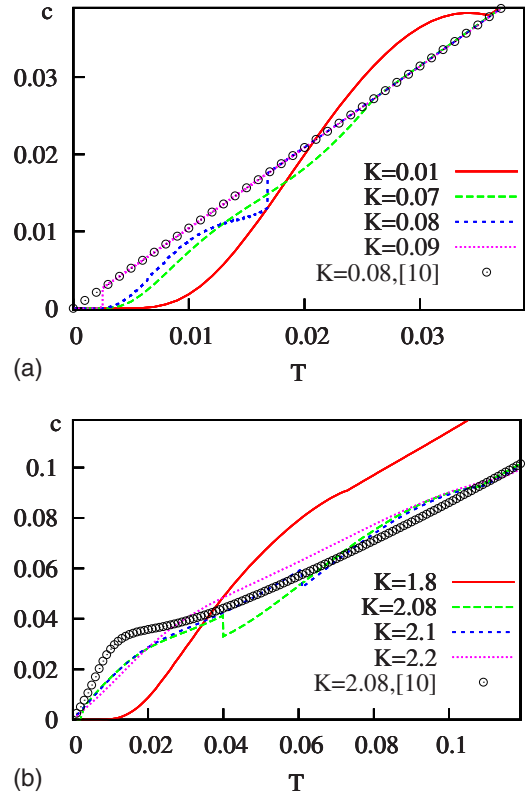


FIG. 16. (Color online) Temperature dependence of the specific heat c for the deformable spin chain ($J=1, \alpha=0.5$) for various values of K . (a) $K=0.01, 0.07, 0.08, 0.09$; (b) $K=1.8, 2.08, 2.1, 2.2$. We also show the results for the rigid spin chain (1) with $J=1, K=0.08$, and $K=2.08$ as they follow from Ref. 10 (open circles).

To summarize this section, the calculated equilibrium properties of the deformable spin chain clearly reflect the changes due to spin-lattice coupling which may give rise to a lattice distortion. We observe an anomalous temperature dependence of such quantities as the static transverse susceptibility or the specific heat. At low temperatures we also observe an anomalous dependence of such quantities as the transverse magnetization on the three-spin coupling constant K , which in turn may depend on external or internal pressure. We believe that our theoretical investigation may be helpful to understand the properties of real spin-Peierls materials for which these equilibrium properties are accessible experimentally.

V. SUMMARY

In this work we study the spin-1/2 XX chain with three-site interactions of $(XZX+YZY)$ type (1) assuming the underlying lattice to be deformable. The deformations of the lattice cause changes in exchange couplings (2). The elastic energy of these static deformations is also taken into account. By constructing trial states we have unambiguously shown that a dimerized or trimerized state has lower ground-state energy and Helmholtz free energy than the uniform state for certain three-site interaction strengths K . Although we cannot exclude that the ground-state energy (for $T=0$) or Helmholtz

free energy (for $T > 0$) can be lowered further by more complicated lattice distortion patterns, our analysis has demonstrated that the uniform chain is unstable in some cases. (We note that rigorous statements about exact distortion patterns of such lattices are rather scarce; for a proof that the dimerized state is the exact ground state for $K=0$ see Ref. 27; some rigorous results about incommensurate patterns are reported in Ref. 28.) The additional three-site interactions considered in our study cause a number of phases to appear in the ground-state phase diagram as compared to the simple nearest-neighbor model. First of all they destroy dimerization, but being sufficiently strong they promote trimerization. As temperature deviates from zero the periodic ground-state phases may first persist but finally disappear. After finding the energetically favorable phases we have calculated some quantities of deformable spin chain (1) considering as examples the dependence of the transverse magnetization m^z on K at different temperatures (Fig. 14) and the temperature dependence of the static transverse susceptibility χ^z and the specific heat c at different K (Figs. 15 and 16). All quantities calculated are visibly influenced by the lattice distortion in the parameter region where the lattice is distorted. Finally, it

should be mentioned that the results reported here may be also of interest in the context of one-dimensional electronic models with next-nearest-neighbor hopping.

In the present paper we focus on the static properties of the model. We notice that an analysis of the dynamic properties of the model requires a separate study [we may mention here a study on dynamic properties of the spin-Peierls transition in simple nearest-neighbor model (1) with $K=0$, i.e., spin-1/2 XX chain,²⁹ as well as some related studies.^{30,31} Another interesting problem which deserves to be examined is the study of the effect of an external (transverse) magnetic field.

ACKNOWLEDGMENTS

This study was mainly performed during our visits in Dortmund and L'viv in 2008, which were subsidized by a NATO collaborative linkage grant under Reference No. CBP.NUKR.CLG 982540. O.D. acknowledges also the kind hospitality of the MIPPKS, Dresden during the seminar Unconventional Phases and Phase Transitions in Strongly Correlated Electron Systems (2008).

-
- ¹A. H. MacDonald, S. M. Girvin, and D. Yoshioka, *Phys. Rev. B* **37**, 9753 (1988).
²D. Sen and R. Chitra, *Phys. Rev. B* **51**, 1922 (1995); R. Chitra and R. Citro, *ibid.* **63**, 054441 (2001).
³J. K. Pachos and M. B. Plenio, *Phys. Rev. Lett.* **93**, 056402 (2004); J. K. Pachos and E. Rico, *Phys. Rev. A* **70**, 053620 (2004); M. S. Tame, M. Paternostro, M. S. Kim, and V. Vedral, *ibid.* **73**, 022309 (2006); D. I. Tsomokos, J. J. Garcia-Ripoll, N. R. Cooper, and J. K. Pachos, *ibid.* **77**, 012106 (2008).
⁴T. Antal, Z. Rácz, A. Rákos, and G. M. Schütz, *Phys. Rev. E* **57**, 5184 (1998); T. Antal, Z. Rácz, A. Rákos, and G. M. Schütz, *ibid.* **59**, 4912 (1999).
⁵A. M. Tselik, *Phys. Rev. B* **42**, 779 (1990); H. Frahm, *J. Phys. A* **25**, 1417 (1992).
⁶M. Suzuki, *Phys. Lett.* **34A**, 338 (1971); M. Suzuki, *Prog. Theor. Phys.* **46**, 1337 (1971).
⁷D. Gottlieb and J. Rössler, *Phys. Rev. B* **60**, 9232 (1999).
⁸P. Lou, W.-C. Wu, and M.-C. Chang, *Phys. Rev. B* **70**, 064405 (2004).
⁹O. Derzhko, J. Richter, and V. Derzhko, *Ann. Phys.* **8**, SI-49 (1999).
¹⁰I. Titvinidze and G. I. Japaridze, *Eur. Phys. J. B* **32**, 383 (2003).
¹¹A. A. Zvyagin, *Phys. Rev. B* **72**, 064419 (2005).
¹²E. Lieb, T. Schultz, and D. Mattis, *Ann. Phys. (N.Y.)* **16**, 407 (1961); S. Katsura, *Phys. Rev.* **127**, 1508 (1962); **129**, 2835 (1963).
¹³P. Pincus, *Solid State Commun.* **9**, 1971 (1971); G. Beni and P. Pincus, *J. Chem. Phys.* **57**, 3531 (1972).
¹⁴J. H. Taylor and G. Müller, *Physica A* **130**, 1 (1985) and references therein.
¹⁵C. E. Zaspel, *J. Chem. Phys.* **86**, 4713 (1987).
¹⁶K. Okamoto, *Solid State Commun.* **83**, 1039 (1992).
¹⁷A. E. Feiguin, J. A. Riera, A. Dobry, and H. A. Ceccatto, *Phys. Rev. B* **56**, 14607 (1997).
¹⁸O. Derzhko and T. Krokhamlskii, *Ferroelectrics* **250**, 397 (2001).
¹⁹Y. Lépine and A. Caillé, *Solid State Commun.* **48**, 769 (1983); M. M. Mohan and Y. Lépine, *Phys. Rev. B* **38**, 11602 (1988).
²⁰J. Zang, A. R. Bishop, and D. Schmeltzer, *Phys. Rev. B* **52**, 6723 (1995).
²¹K. Okamoto and T. Nakamura, *J. Phys. A* **30**, 6287 (1997).
²²S. Hirata and K. Nomura, *Phys. Rev. B* **61**, 9453 (2000).
²³O. Derzhko, T. Krokhamlskii, J. Stolze, and T. Verkholyak, *J. Phys.: Conf. Ser.* (to be published).
²⁴A. A. Zvyagin and G. A. Skorobogat'ko, *Phys. Rev. B* **73**, 024427 (2006).
²⁵E. Jahnke, F. Emde, and F. Lösch, *Tables of Higher Functions* (B. G. Teubner Verlagsgesellschaft, Stuttgart, 1966), p. 62.
²⁶T. Krokhamlskii, O. Derzhko, J. Stolze, and T. Verkholyak, *Acta Phys. Pol. A* **113**, 437 (2008); T. Krokhamlskii, O. Derzhko, J. Stolze, and T. Verkholyak, *Phys. Rev. B* **77**, 174404 (2008).
²⁷T. Kennedy and E. H. Lieb, *Phys. Rev. Lett.* **59**, 1309 (1987).
²⁸S. Brazovskiy and I. Dzyaloshinsky, *J. Stat. Phys.* **38**, 115 (1985).
²⁹K. Kawasaki, N. Maya, A. Kouzuki, and K. Nakamura, *J. Phys. Soc. Jpn.* **66**, 839 (1997); A. Kouzuki, K. Kawasaki, and K. Nakamura, *Phys. Rev. B* **60**, 12874 (1999).
³⁰I. Harada, S. Mori, and N. Ohtsuka, *J. Magn. Magn. Mater.* **177-181**, 665 (1998); S. Mori, I. Harada, and T. Tonegawa, *J. Phys. Soc. Jpn.* **67**, 1409 (1998).
³¹M. Müller and H.-J. Mikeska, *J. Phys.: Condens. Matter* **12**, 7633 (2000).